Available online at www.sciencedirect.com
ScienceDirect
Journal of Photochemistry and Photobiology A: Chemistry 189 (2007) 286–294
Journal of Photochemistry and Photobiology A:Chemistry
www.elsevier.com/locate/jphotochem

Photoactive TiO_2 films on cellulose fibres: synthesis and characterization

M.J. Uddin, F. Cesano, F. Bonino, S. Bordiga, G. Spoto, D. Scarano, A. Zecchina *

Nanostructured Interfaces and Surfaces (NIS), Centre of Excellence, Department of Chemistry IFM, University of Turin, Via P. Giuria 7, I-10125 Torino, Italy

Received 22 December 2006; received in revised form 12 February 2007; accepted 15 February 2007
Available online 23 February 2007

Abstract

The preparation of photoactive fibres has been successfully developed by depositing and grafting TiO_2 nanoparticles on cellulose fibres by using a sol–gel method at low temperature (∼100 °C)—designed for practical applications. The original and treated fibres have been characterized by several techniques (SEM, HRTEM, FTIR, Raman, UV–vis spectroscopy, XRD, and TGA). The TiO_2 nanoparticles, 3–5 nm in size, have been found to form a homogeneous thin film on the fibre surface, which shows efficient photocatalytic properties when exposed to solar-like light. The photocatalytic activity, tested by measuring the degradation of adsorbed methylene blue (MB) and of a heptane-extracted bitumen fraction (BF) containing a mixture of heavy aromatic hydrocarbons, is fully maintained upon several numbers of impregnation–photodegradation cycles. The fibre structure is not altered upon light exposure. The TiO_2 film is firmly anchored and the photocatalytic activity is retained even after 20 washing cycles. This preparation technique can be also applied to new fabrics to create self-cleaning and UV irradiation protection properties in them.

Keywords: Photocatalysis; Cotton–TiO_2 composite fibres; Methylene blue (MB); Heptane-extracted bitumen fraction (BF); Spectroscopic and microscopic techniques

1. Introduction

Titanium dioxide, an inexpensive, non-toxic and biocompatible material, is one of the most important and widely investigated photocatalysts [1], because of its potential application in decomposition of various environmental pollutants in both gaseous and liquid phases [2]. Development of TiO_2 based photocatalysts anchored to supporting materials with large surface areas, where pollutants could be condensed, would be of great significance, not only to avoid the disadvantages of filtration and suspension of fine photocatalyst particles, but also to lead a high photodecomposition efficiency [3]. Photocatalytic degradation on TiO_2 of many substances (4-chloro-2-methylphenol [4], gaseous alcohols [5], isothiazolin-3-ones [6], formaldehyde [7], 3-amino-2-chloropyridine [8], acid orange [9], phenol, 4-chlorophenol, 2,5-dichlorophenol, 2,4,5-trichlorophenol, 1,3,5-trihydroxybenzene, 2,3-dihydroxynaphthalene [10a] and diuron on flexible industrial photoresistant paper [10b]) was studied under various illumination conditions. Among these, photocatalytic disinfections of *Escherichia coli* on TiO_2 was studied by Lincon et al. [11] and Li et al. [12], who ascribed the bioactivity of the titania layers to the presence of hydroxyl (OH) groups and to a negatively charged surface. A novel method for the processing of sol–gel derived titanium dioxide composites has been developed and investigated for the purpose of producing thick films and self-supported photocatalysts. The resulting photocatalyst exhibits relatively high surface area and enhanced mechanical stability and integrity [13]. Furthermore, when compared with silicatitanate [14] or SiO_2–TiO_2 photocatalysts [15], TiO_2 appears more efficient. It is known that both the optical properties and the photocatalytic activity of TiO_2 coatings depend strongly on the phase, the crystallite size and the porosity of the coatings [16]. In our previous work [10a] we have described (a) the role of surface structures in influencing the photocatalytic activity and selectivity with the aim to bring new information on the activity of internal and external sites; (b) the effect of altering the excitation frequency and hence the ratio between the contribution of the band gap and charge-transfer mechanisms on the photocatalytic processes. Recently, several studies on the different nucleation processes of anatase TiO_2, at relatively low temperatures, have been published. Among these the following processes can be highlighted

* Corresponding author. Tel.: +39 011 6707860; fax: +39 011 6707855.
E-mail address: adriano.zecchina@unito.it (A. Zecchina).

1010-6030/$ – see front matter © 2007 Elsevier B.V. All rights reserved.
doi:10.1016/j.jphotochem.2007.02.015

to obtain: (a) TiO_2 nanocrystalline thin films by exposing to boiling water [17], (b) TiO_2–SiO_2 films under water vapor exposure at 60–180 °C [15], (c) anatase nanocrystals deposited on cotton fabrics from titanium isopropoxide (TIP) solutions, at $T \leq 100$ °C by sol–gel process, with hydrothermal treatment [18] and, more recently, (d) bleached and mercerized cotton textile fibres activated by RF or MW-plasma and UV-irradiation. As far as procedure (d) is concerned, the objective was to introduce negatively charged functional groups which are known to interact with the TiO_2 colloids to anchor TiO_2 on cotton textile [19].

The aims of our study are: (a) to develop a simple and repeatable anchoring procedure of the TiO_2 nanophase to the cellulose fibres, (b) to perform accurate characterization of the structure and properties of the composite obtained by means of sol–gel technique, (c) to check photostability of the TiO_2 film and of the supporting cellulose fibre upon prolonged exposure to light, (d) to investigate the photodegradation of kinetics and (e) to check the reuse of the TiO_2-covered fibres for multiple pollutant adsorption–photodegradation cycles. The preparation method is novel because an organic amine was used in the sol to stabilize the solution for long time. It is a matter of fact that the resulting TiO_2 containing transparent sol was quite stable up to a long time. In our lab, the sol was stable without opacity up to 7 days. This innovation is important because it should allow its practical use for industrial applications. In fact, the use of the same sol for multiple times is simplifying the impregnation procedure. To the best of our knowledge, this is a new development of processing method. The photocatalytic activity of nanocrystalline TiO_2-modified cellulose fibre, prepared at low temperatures, was monitored by measuring the photocatalytic degradation of adsorbed methylene blue (MB) and of adsorbed bitumen fraction extracted with heptane (BF) composed of high molecular weight hydrocarbons with high aromatic character. This photocatalytic activity was compared with that observed from untreated fibres. The choice of MB as pollutant is quite conventional since this molecule is normally used to test the photoactivity of TiO_2-based materials. The use of a bitumen fraction extracted with heptane is less common. This choice finds explanation in the need to verify the activity of our system in the photodegradation of a completely different class of molecules. To control the potential photodegradation effect in the presence of supported TiO_2 particles not only on the adsorbed species but also on the cellulose support, the IR spectra of the cotton fibre at increasing times of exposure to the light has been monitored. The stability of the photocatalyst upon 20 washing cycles has also been investigated.

2. Experimental

2.1. Materials

Pure cellulose fibre characterized by 10–15 μm diameter, from Cotton PVS srl (Segrate, Italy), was used for the entire process. All chemicals were from Aldrich, Germany and used as received. The water used in our experiments was triply distilled and produced in our laboratory.

2.2. Method

The fibre samples were treated with acetone for 30 min in a Soxlet chamber to remove impurities like wax, fat, etc. and dried at room temperature for 12 h. Titanium isopropoxide (TIP) was used as a precursor of TiO_2. A solution was prepared as follows: TIP (0.02 mol) was added to 2-isopropanol (50 ml) under vigorous stirring conditions and then triethyl amine (0.01 mol) was added as a stabilizer of the solution and stirred (200 rpm) for 2–3 min under an inert environment. The required inert environment was made by argon gas flow through the system. A second solution was then prepared separately as follows: hydrochloric acid (3.0 ml) and water (0.72 ml) were added to 2-isopropanol (50 ml) and mixed well by a magnetic stirrer (200 rpm). The two solutions were then mixed together and stirred vigorously for 30 min under Ar gas flow. The formed TiO_2 sol was transparent, quite stable and highly sensitive to the amount of triethylamine and water. For the impregnation, the cellulose fibres after being dried in a preheated oven, as described before, are then immersed for 30 s in the TiO_2 containing liquid sol. The extracted samples were then placed in 70 °C preheated oven to remove the solvent from the fibre and then heated at 95 °C for 5 min, to complete the formation of titanium dioxide from the precursor. Finally, the impregnated fibres were treated in boiling water for 3 h (post curing). During this step the unattached TiO_2 particles were removed from the fibre surface. A second sample was obtained by treating the cellulose fibres in the same way, except from the TiO_2 impregnating phase.

2.3. Characterization techniques

To investigate the morphology of the pure and TiO_2-modified cellulose fibres, SEM (scanning electron microscopy) images were obtained on a SEM instrument (Leica, Stereoscan 420) equipped with energy dispersive spectroscopic (EDS) microanalysis system (OXFORD). Bulk EDS analysis was also performed to verify the elemental composition of the deposited materials on the fibre surface. The TiO_2 particle sizes were obtained by high-resolution transmission electron microscopy (HRTEM) (JEOL 2000EX instrument, 200 keV).

The UV–vis reflectance spectra were carried out at room temperature on a Perkin-Elmer UV–vis–NIR spectrometer to detect UV absorption intensities, the location of absorption edges and the quantum size effects (if any) of the photocatalyst [20]. The UV–vis spectra have been obtained in the reflectance mode on the dried samples. This procedure is aimed to avoid systematic errors in evaluating the intensities of the specific UV–vis bands of the absorbates, because, as it is known, different fillings of the intra-crystalline voids by the solvent molecules have an important effect on the scattering properties of the samples [21].

XRD patterns have been collected by means of a Philips PW1830 X-ray diffractometer in a Bragg Brentano configuration to identify the crystal phase and structure. Co Kα radiation beam with 40 kV and 20-mA, has been used. The observed patterns have been analyzed using Philips X'Pert High Score software and compared with standard patterns of International Center of

Diffraction Data (ICDD) and Powder Diffraction File (PDF) data bases.

To analyze the cellulose polymer chain quality before and after the treatment and also after long-time exposure to solar-like light, FTIR analysis was performed on the samples mixed with KBr. The spectra were recorded with a IFS66 spectrometer equipped with a MCT cryodetector at a resolution of 2 cm^{-1}. Raman spectra were recorded with a Renishaw in Via Raman Microscope spectrometer equipped with Ar^+ laser beam emitting at 514 nm, at 8.2 mW output power. The photons scattered by the sample were dispersed by a 1800 lines/mm grating monochromator and simultaneously collected on a CCD camera; the collection optic was set at 50× objective.

To investigate the quantity of TiO_2-deposited film thermogravimetric analysis was performed in air flow (ramp of 5 °C/min) by Universal 2050 TGA V5.4A instrument.

2.4. Photocatalytic degradation

The photoactivity of the titanium dioxide coated cellulose fibres has been investigated by exposing the samples containing adsorbed methylene blue (MB) and heptane-extracted bitumen fraction (BF) to solar-like light. For photocatalytic reactions, the irradiation was carried out on dry sample at 308 K, using a SOL2/500S lamp (honle UV technology, Munchen, Germany) simulating solar light. The SOL-bulb and the H_2 filter together yield a spectrum very similar to the natural sunlight, ranging from ultraviolet to infrared radiation (approx 295–3000 nm). For this purpose, aqueous solutions (0.05%, w/v) of reagent grade MB and non-aqueous solution of BF (0.2%, w/v) were prepared for impregnation of the pure and of TiO_2-covered cellulose fibres. The same amount of each sample was immersed under mild stirring in the same amount of the solution and remained overnight to complete the adsorption. The solution was then removed and the samples dried at room temperature. From the decrement of MB and BF in solution, the concentration on the fibre was estimated to be 3.9 mg/g cellulose and 2.3 mg/g cellulose, respectively. The so-obtained samples were then exposed to reproducible solar like light (50 mW/cm^2) to test their photoactivity. The photodecomposition reaction was monitored with a UV–vis spectrometer in the reflectance mode by investigating the evolution of the absorbance upon light exposure. *In situ* UV–vis reflectance method used to follow the degradation of MB is novel and never used. The adsorption and the photocatalytic degradation cycles were repeated three times on the same sample to check the photostability.

3. Results and discussion

3.1. SEM, HRTEM images and EDS analysis of TiO_2 coatings

In order to investigate the morphology of the obtained samples, comparison between the SEM images of the treated and untreated cellulose fibres is illustrated in Fig. 1a–d. From Fig. 1b the presence of folds running parallel to the elongation direction

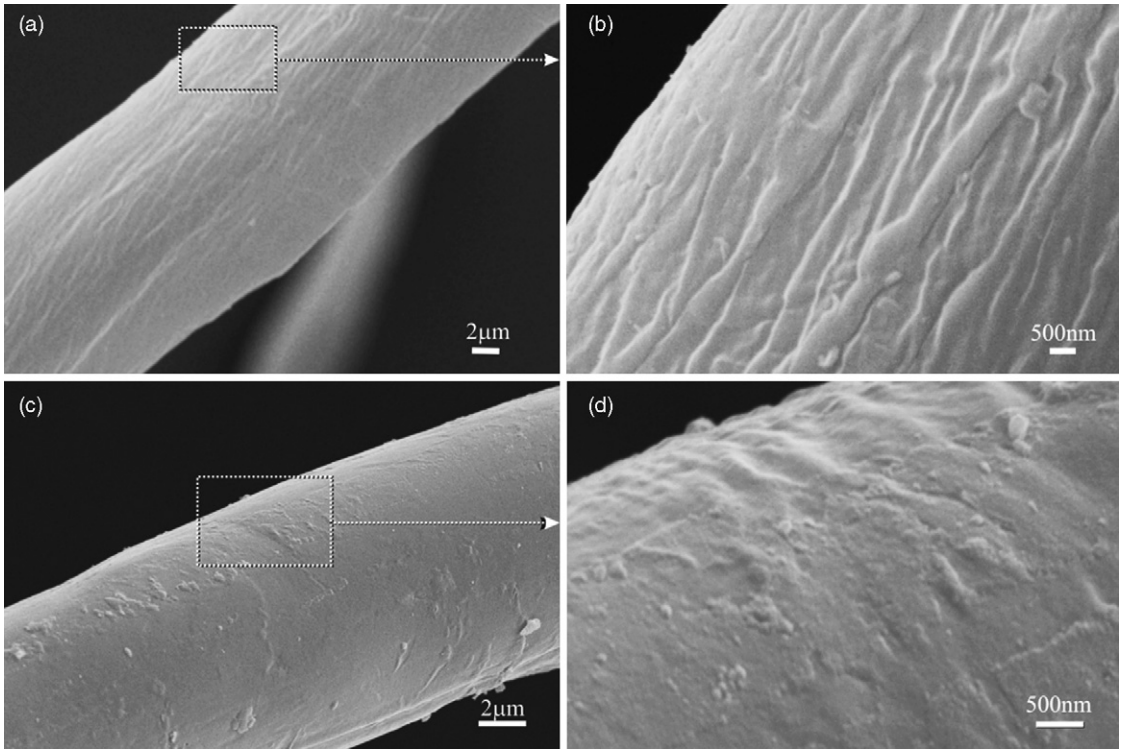

Fig. 1. SEM images of: (a) pure fibre, (b) enlarged view of the selected area in (a), (c) TiO_2-coated fibre, (d) enlarged view of the selected area in (c). In the first two pictures, the presence on the surface of folds quite parallel to the fibre axis, is evident. Pictures (c) and (d) show the presence of a TiO_2 coating, which covers homogeneously the surface of the fibres, whereas the presence of folds is not more evidenced. Rare and large TiO_2 nanocrystals aggregates, emerging from the fibre coating, are identifiable at the adopted resolution.

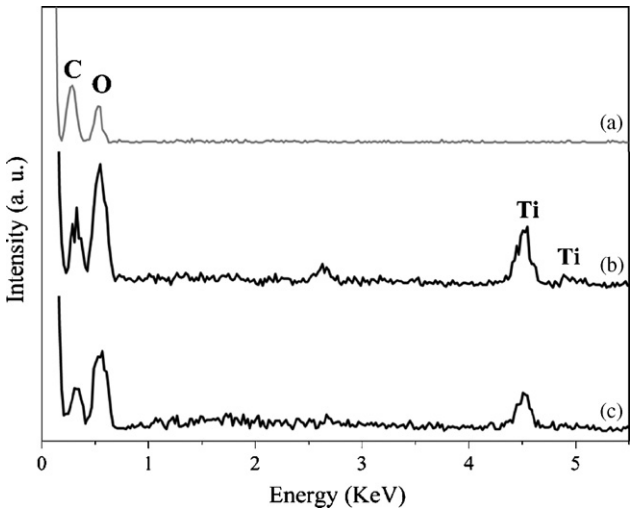

Fig. 2. EDS spectra of: (a) pure fibres, shown as a reference (solid grey line), (b) TiO_2-coated cellulose fibres before washing, (c) TiO_2-coated cellulose fibres after 20 washing cycles by liquid detergent.

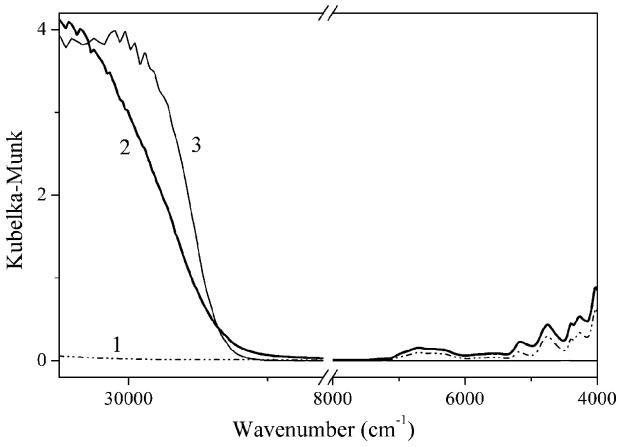

Fig. 4. UV–vis reflectance spectra of: (1) pure fibres (dot dot dashed line), (2) TiO_2-covered fibres and (3) pure TiO_2 anatase. The bands in the 8000–4000 cm^{-1} range have vibrational origin because they are combination and overtones of cellulose modes.

of the fibre, is imaged. Otherwise, Fig. 1c and d clearly show that treated fibres are covered by a continuous and homogeneous TiO_2 thin film, which obscures the surface folds below. In addition, the presence of rare aggregates of TiO_2 particles can be single out on TiO_2-covered fibres. In Fig. 2 the EDS analysis of pure cellulose fibres (a), TiO_2-covered fibres before washing (b) and after washing (c) are reported. On the basis of these results, it is noteworthy to observe that (i) the deposited material consists of titanium and oxygen (Fig. 2b and c); (ii) after 20 washing cycles, remarkable amount of titania is still present on the cellulose surface (Fig. 2c). This means that TiO_2 particles are firmly anchored to the surface of fibres. The continuous and homogeneous nature of the TiO_2 films suggests that pollutant molecules impinging the fibre–TiO_2 composite will interest preferentiably with the TiO_2 phase covering the fibres (*vide infra*).

In order to determine in more detail, the nanometric structure and the morphology of the TiO_2 particles forming the film, a portion of material was collected by scratching the thin film surface and analyzed by HRTEM. TEM images, reported in Fig. 3, show that the deposited titania film consists of particles almost uniform in size (3–5 nm). It is remarkable that the particle size and morphology of the deposited titania on the fibre surface are uniform through the entire surface. The data concerning the particle size will be supported by the XRD, UV–vis and Raman data (*vide infra*). This differentiates our TiO_2 surfaces from similar surfaces obtained by TiO_2 deposition on glass substance [22], silica gel [23], steel plate [24] and ceramic membranes [25]. The small dimension of the TiO_2 particles suggests that the exposed surface area of TiO_2 film is very large. This fact together with the above-mentioned continuous character of the film is at the origin of the preferential adsorption of the pollutant on the external layers as it will be detailed in the following. This uniform layer of supported TiO_2 is likely the prerequisite allowing the photocatalytic degradation of the pollutant without aggression of the underlying cotton fibre.

3.2. UV–vis reflectance spectra

Fig. 4 shows the reflectance spectra of pure cellulose fibres (curve 1), of TiO_2-covered fibres (curve 2) as compared to the spectrum of anatase TiO_2, used as reference (curve 3). An absorption edge at 29,000 cm^{-1} (curve 2), which is slightly upward shifted with respect to that of pure anatase TiO_2

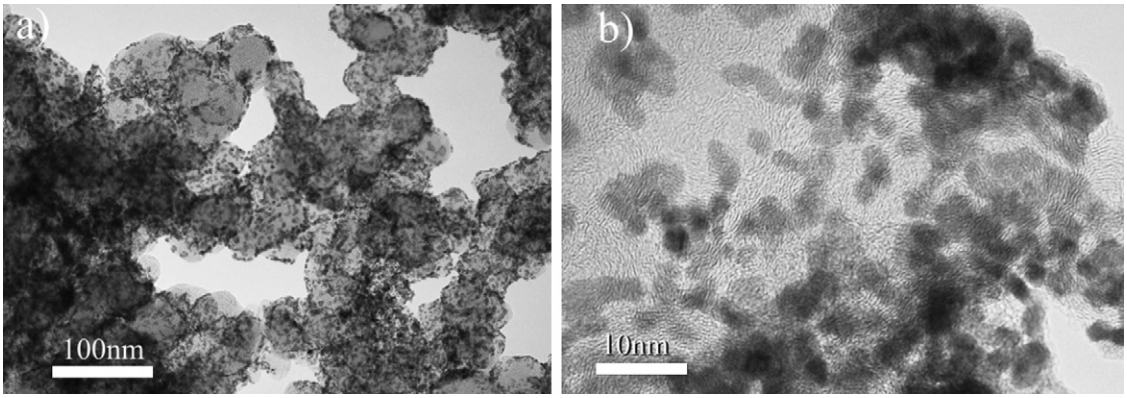

Fig. 3. TEM images of: (a) portion of the TiO_2-coated fibres, (b) HRTEM image of a selected area in (a). The high resolution image shows a low density region, with TiO_2 nanoparticles 3–4 nm in size.

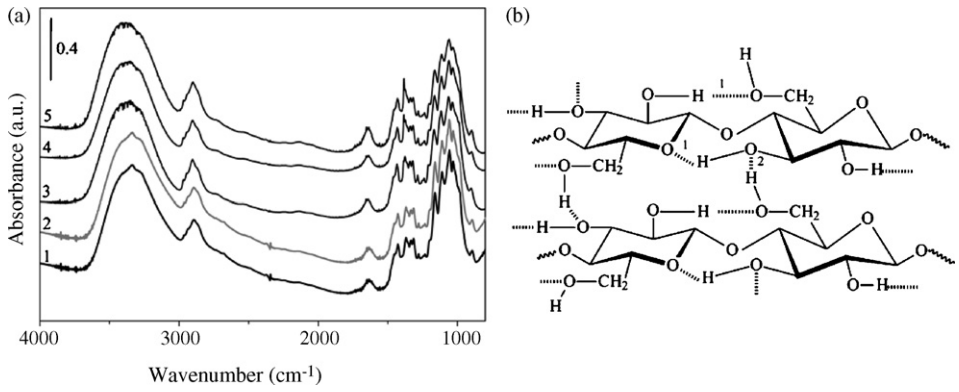

Fig. 5. (a) FTIR spectra of: pure cellulose fibres (1), TiO_2-covered fibres (grey curve) (2), cellulose fibre upon 24 h (3), 48 h (4) and 84 h (5) of solar light exposure. Spectra 2–5 shows fibre stability upon treatment and solar like light exposure. (b) Scheme of a cellulose fibre structure (1 and 2 denote the intra- and inter-chain H-bondings, respectively).

(curve 3), is indicative of the presence of the anatase phase TiO_2. This absorption edge, of course, is absent in the curve 1 corresponding to the pure cellulose fibres. The observed blue shift of the absorption edge on the TiO_2-covered fibres with respect to pure TiO_2 (P25) is due to quantum size effects typical of small particles, which have a higher band gap with respect to that of infinite crystals. This observation is qualitatively confirming the SEM and HRTEM results. However even very small TiO_2 nanoparticles are strongly bounded to the fibres infact the observed good stability toward washing suggests that the anchoring process of the particles involves the formation of chemical bonds, for example via esterification of the surface OH groups with titanols.

As far as photocatalytic properties are concerned, it is known that, due to the electronic structure of titanium dioxide, optical photons with energy matching or exceeding its band gap energy can be absorbed with formation of electrons and holes [26] (band gap mechanism). Consequently, the TiO_2 film can act as photocatalyst under UV-irradiation. However, as discussed in [10a], this is not the only photocatalytic mechanism observed on TiO_2. In fact, a charge-transfer mechanism can also be operative under visible light irradiation.

3.3. FTIR and Raman spectra

In Fig. 5, the IR spectra of the cellulose fibres before and after TiO_2 grafting are compared (curves 1 and 2). The aim of the experiment was to ascertain whether IR spectroscopy could be informative on the grafting mechanism, which is expected to involve the esterification of OH groups located on the external surface of the fibres. The spectrum of the virgin sample (Fig. 5, curve 1) is characterized by an intense and broad band in the 3600–3100 cm^{-1} range, associated with inter- and intra-chain OH–O groups (τ) of the interacting chains as reported in Fig. 5b. A peak at ~1600 cm^{-1} is also indicative of the presence of interstitial or adsorbed water. The absorptions in the 3000–2800 and 1450–1350 cm^{-1} ranges are due to the ν(CH) and δ(CH) modes. Finally, the complex absorption in 1250–900 cm^{-1} range is mainly associated with stretching mode of C–O–C groups of the fibre framework. All the above-mentioned groups are mainly located inside the films. Due to the diameter of the fibres (~10 μm) the contribution of the external alcoholic groups, which are expected to actively participate in the anchoring process and hence to be consumed by the grafting procedure, is expected to be small or in the worse case, negligible. This is demonstrated by the spectrum of the fibres after grafting (Fig. 5, curve 2), which is substantially unaltered. This means that due to the low external surface area of the supporting fibres, the IR spectroscopy is not informative on the grafting mechanism at all. It is quite remarkable that being the IR spectrum of the treated sample totally dominated by the spectrum of the fibre, the contribution of the TiO_2 phase (which should appear at $\bar{\nu} < 700\ cm^{-1}$) is also negligible. The photostability of the cellulose fibres is illustrated in Fig. 5, where the curves 3–5 correspond to the sample exposed to solar-like light for 24, 48, 84 h, respectively. It can be seen that the absorption band at ~3400 cm^{-1} and the complex absorption in the range 1650–1050 cm^{-1} characteristic of the fibres are mostly unchanged. These three curves indicate that the chemical structure of cellulose fibre is not substantially altered upon exposure to solar-like light. In our opinion this is due to the homogeneous character of TiO_2 film which completely adheres and protects the fibres from aggression of O_2^- and $OH^\bullet$ species generated during the exposure to the light.

A more useful piece of information on the vibrational frequencies of the external Ti-rich layers of the TiO_2-covered fibres comes from Raman spectra of the two above-mentioned samples (i.e. virgin and treated) (Fig. 6). It can be immediately seen that the spectrum of the treated samples (curve 2) is dominated by new peaks (at 157, 199, 404, 517, and 640 cm^{-1}) associated with TiO_2 phase. Comparison with the Raman spectrum of pure anatase TiO_2 (curve 3), which shows band at 143, 196, 396, 515, and 639 cm^{-1}, demonstrates that the surface layer is mainly constituted by anatase. Conversely, Raman spectrum of pure cellulose fibres treated with blank sol, shows no peak at all regarding TiO_2 (curve 1). In conclusion, unlike IR, Raman spectroscopy shows its utility to reveal the presence of TiO_2 particles on the external surface of the films. It is useful to underline that the Raman peaks of the supported TiO_2 are much broader than those of the pure anatase. A few expla-

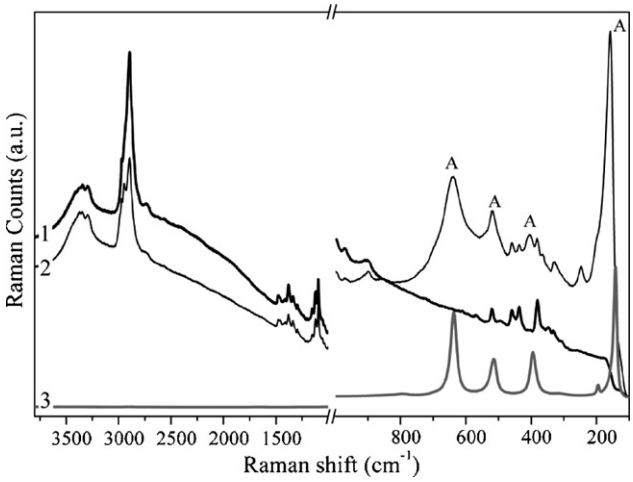

Fig. 6. Raman spectra of: pure cotton fibres (1), TiO_2-covered fibres TiO_2 (2) and pure TiO_2 anatase (grey curve) (3).

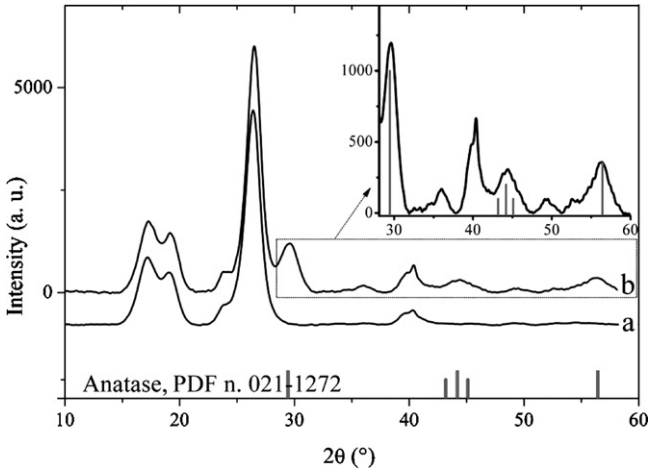

Fig. 7. XRD patterns of: (a) pure and (b) TiO_2-covered fibres. The gray vertical lines superimposed to XRD patterns represent the peak positions of the standard anatase (PDF no. 021-1272). In the inset an exploded view of a selected region of the XRD pattern is shown.

nations can be argued to explain the increase of the peak half width. For instance, Raman studies of nanosized anatase phase TiO_2, produced by sol–gel route at low temperatures (i.e. lower than 100 °C), show that the Raman spectrum of TiO_2 is slightly dependent upon the particle size and upon crystallinity. In particular, particles having small dimension and low crystallinity are characterized by Raman peak broadening. It is noticeable that our Raman spectra closely resemble those previously described [14] for TiO_2 samples, obtained by hydrolysis of titanium isopropoxide and calcination in the 70–300 °C temperature range, which are all characterized by particles with diameter lower than 5 nm. Another interesting observation concerns the position of Raman band at 157 cm^{-1} which is distinctly upward shifted with respect to that of the pure anatase. Choi et al. [27] suggested that the Raman bands shift towards higher wavenumbers as the particle size decreases. In particular, when the particle size decreases to the nanometer scale, the lowest Raman band shifts towards a higher wavenumber due to the increasing force constants [28,29]. As a similar shift is observed on our sample, we conclude that Raman spectroscopy reveals its utility in giving information on the presence of a TiO_2 nanostructured layer constituted by small nanoparticles (≤5 nm) and confirms the results derived from SEM, HRTEM and UV–vis characterization techniques. However it must be concluded that, like IR, Raman spectroscopy does not give additional information on the anchoring mechanism.

3.4. X-ray diffraction (XRD) analysis

The XRD patterns of pure and titania-coated cellulose are reported in Fig. 7. In the inset, an exploded view of the pattern of the TiO_2 impregnated sample is shown together with the position of the peaks of anatase taken from the reference. Curve (a) reports two broad peaks and one intense peak at 17.21°, 19.143° and 26.40°, respectively, which constitute the typical XRD pattern of cellulose fibres [30]. Curve (b) shows broad peaks at 29.41°, 44.20° and 56.40° which are closely related to anatase phase. No additional peaks belonging to other phases are observed. The remarkable width of the peaks associated with the TiO_2 phase suggests that the size of the particle is quite small. From full width at half maximum (FWHM) of the peaks at 29.41° and 56.40° and by using Scherrer's equation, $Lc = K\lambda/(\beta \cos\theta)$ [31] (where λ is the X-ray wavelength, β is the FWHM of the diffraction line, θ is the diffraction angle, and K is a constant, which has been assumed to be 0.9), an average particle diameter of about 5 nm, can be calculated. This result is strongly consistent with the SEM, HRTEM, UV–vis and Raman results described above. In conclusion, by comparing the results coming from the different techniques, it comes out that the investigated cellulose samples contain nanosized anatase particles of uniform size (≤5 nm).

3.5. TGA analysis

The TGA analysis of the cellulose fibre carried out in air, in heat flow response, shows two major exothermic peaks (Fig. 8),

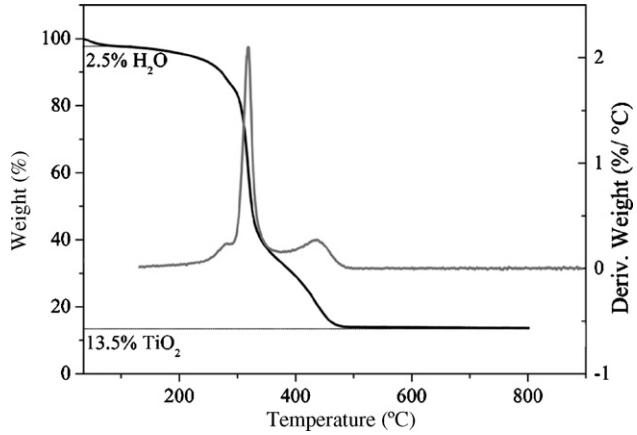

Fig. 8. TGA (black) and DTGA (grey) curves of the TiO_2-coated fibres (ramp 5 °C/min, 35–900 °C, in air). The residual weight of the sample, recorded at 900 °C, is related to the TiO_2 content, after that the cellulose fibre burning has taken place.

in agreement with literature data [32,33]. An unified weight decrease (∼2.5%) is associated with water desorption. After combustion of all organic part, the residual amount (13.5% by weight) corresponds to TiO_2. From this result, it is evident that the TGA technique in air allows to directly evaluate the amount of TiO_2 covering the cellulose fibres, as obtained by the synthesis procedure described before.

3.6. Visible light photocatalysis

The photocatalytic activity of TiO_2-covered cellulose fibres was carried out, as follows: a solutions of either methylene blue (MB) or of a bitumen fraction extracted with heptane (BF) were contacted with the treated and untreated fibres, respectively. After adsorption of MB or BF, the fibres were dried at room temperature. Under this condition, of course, some adsorbed water is remaining as confirmed by IR spectra previously reported in Fig. 5a. The UV–vis reflectance spectra obtained on the dried samples before (curve a) and after illumination (curves b–f and b–d) are reported in Fig. 9a (reactivity toward MB) and c (reactivity toward BF), respectively. From Fig. 9a, it can be observed that the complex absorption bands in the 20,000–12,000 cm^{-1} interval due to adsorbtion of MB, change rapidly because supported TiO_2 promotes the catalytic photodegradation (curves b–f). This is not unexpected since the photocatalytic activity of TiO_2 is well known [34–37]. The disappearance rate of the band due to MB adsorbed on the TiO_2-covered fibres is much higher than that observed in case of untreated fibres. On the basis of the data reported in the literature [38–40], the bands at 15,400 and 16,400 cm^{-1} are assigned to the monomeric and aggregated MB (mostly dimeric and trimeric species) adsorbed on the surface. Under light exposure the aggregate species disappear

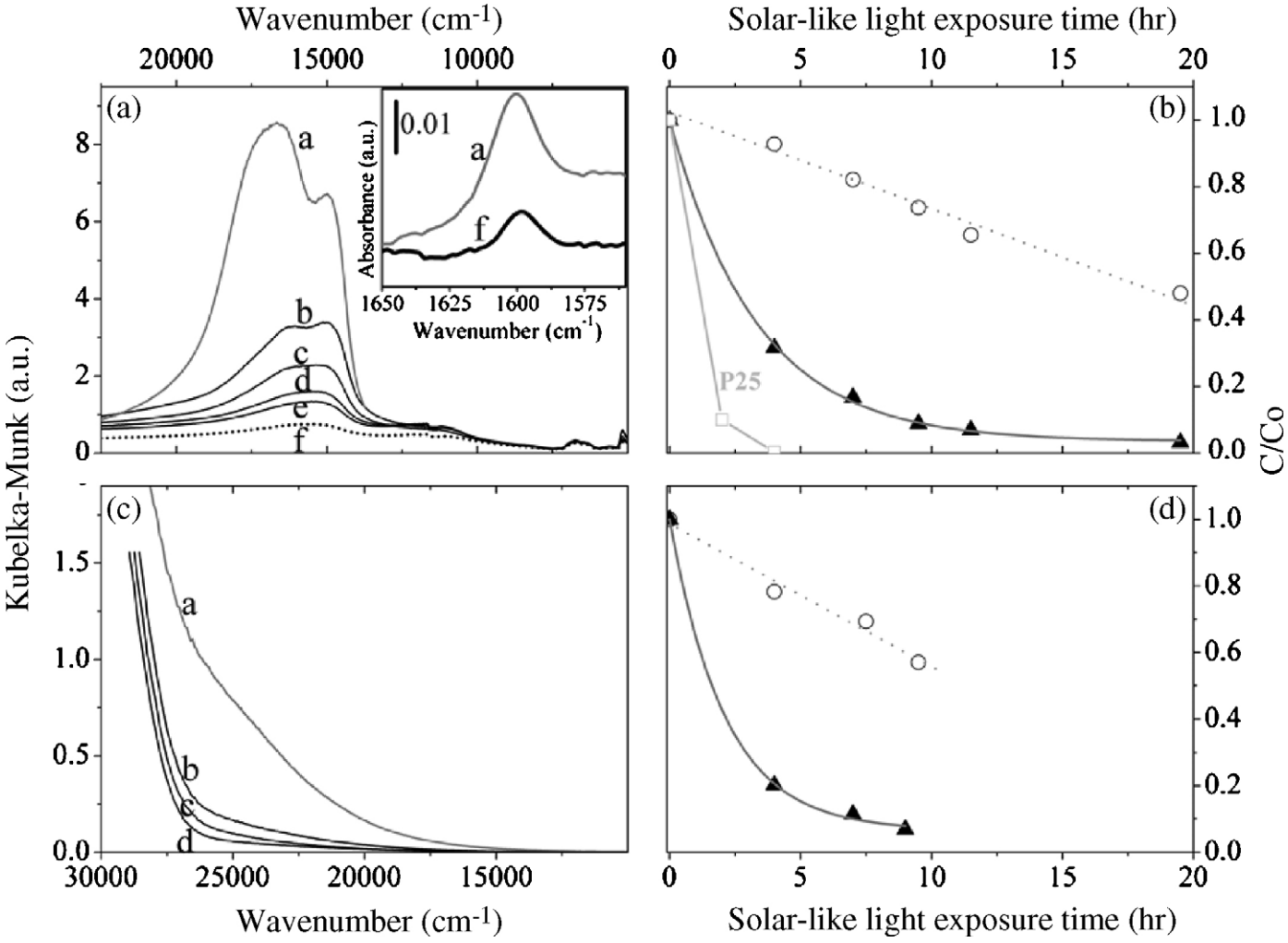

Fig. 9. (a) UV–vis spectral changes of methylene blue (MB) on TiO_2-coated fibres as a function of time of exposure at room temperature, under artificial solar irradiation: no exposure (curve a), irradiation for 4 h (curve b), 7 h (curve c), 9.5 h (curve d), 11.5 h (curve e) and 19.5 h (curve f); in the inset of (a), the decrement, upon irradiation, of the 1600 cm^{-1} band of adsorbed MB is illustrated: (a) before irradiation, (f) after irradiation (each spectrum here reported has been obtained by subtracting the spectrum of the pure cellulose fibres for clearance). (b) Time dependence of the surface concentration of adsorbed MB upon light exposure. Photocatalytic activity of TiO_2-coated fibres (▲), untreated fibres (◯) and P25 (□) on MB. (c) UV–vis spectral changes of the spectrum of heptane-extracted bitumen fraction (BF) adsorbed on TiO_2-coated fibres as a function of time of exposure at room temperature, under artificial solar irradiation: no exposure (curve a), irradiation for 4 h (curve b), 7 h (curve c), 9.5 h (curve d). (d) Time dependence of the surface concentration of adsorbed BF upon illumination. Photocatalytic activity of TiO_2-coated fibres (▲) and untreated fibres (◯).

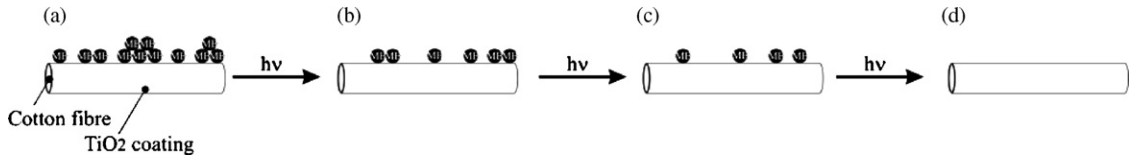

Scheme 1. Photodegradation steps of MB on a TiO_2/cellulose fibre composite starting material (a). Monomeric and polymeric species of MB are simultaneously present on the coated fibre before the light exposure (b). Upon direct light irradiation of the fibres, aggregated species disappear first. At longer exposure time only monomer MB is present (c), before the fibre becomes completely cleaned (d).

first, followed by the monomeric ones. The photodegradation process can consequently be represented to proceed as follows (Scheme 1).

Of course the photodegradation effect is lower than that observed on P25 (Fig. 9b), which is the best TiO_2 catalyst. The photodegradation process can be followed also by the gradual disappearance of the IR bands of adsorbed MB. Among all bands of MB, that at 1600 cm^{-1} can be better monitored, since it falls in a region where the cellulose skeleton is not adsorbing. The results are shown in the inset of Fig. 9a. It is worth noticing that both UV–vis and IR spectroscopies were unable to clearly reveal the formation of intermediate degradation products during the photocatalytic process. For this reason we do not speculate about the detailed degradation mechanism.

Similar results have been obtained for the adsorbed BF (Fig. 9c). As a matter of fact the adsorption (shoulder at 25,000 cm^{-1} with a tail extending up to 15,000 cm^{-1}) decreases rapidly under the exposure to light. Fig. 10(a) shows that the photocatalytic efficiency of the TiO_2-coated fibre on degradating MB is unchanged upon repeating cycles. Moreover, the reaction efficiency is slightly increasing from the first cycle to the second and the third one. A similar stain removal efficiency is obtained in the case of adsorbed BF as shown in Fig. 10(b). These results suggest that TiO_2 losses from the fibre surface for each impregnation of stains (MB and BF) are ignorable and this is in agreement with the results shown in Fig. 2. It is known that the degradation of the stains by UV/TiO_2 process is enhanced for samples in equilibrium with a humid atmosphere [37]. On these basis we argue that the general photoactivity displayed towards the hydrophobic bitumen fraction suggests that adsorbed water (see Fig. 5a) presumably bonded via hydrogen bonds to alcoholic groups type OH, is playing a favourable role. It is worth noticing that the photocatalytic efficiency of the TiO_2 films composite is higher for the adsorbed bitumen fraction than for MB. An interpretation of this result is difficult and it is not representing the scope of this paper. We only argue that unlike MB, the adsorption band of the adsorbed bitumen fraction is partially overlapping the TiO_2 adsorption edge. A dependence of the photodegradation ability upon the matching of the TiO_2 conduction band with the LUMO level of the adsorbed molecule (band alignment) has been already observed [10a].

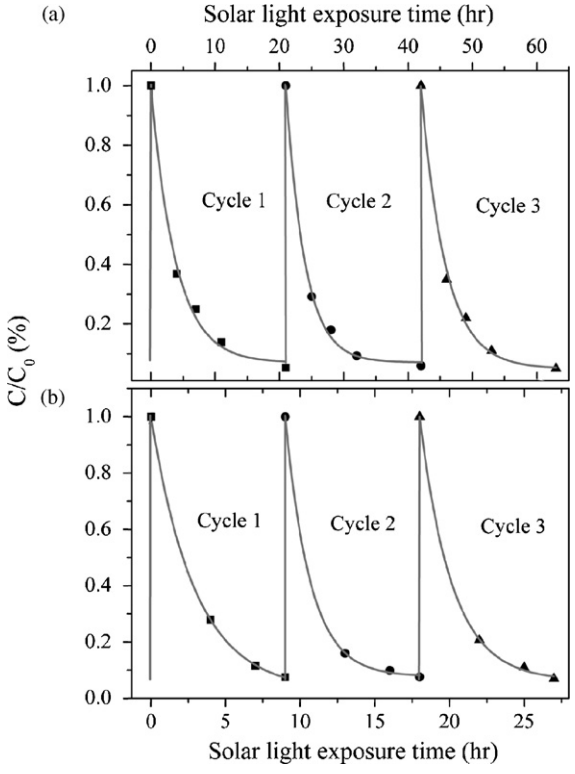

Fig. 10. (a) Photocatalytic activity of TiO_2-covered cellulose fibre upon repeated MB adsorption–illumination cycles. (b) Photocatalytic activity of TiO_2-covered cellulose fibre upon repeated BF adsorption–illumination cycles.

From all these data, it is evident that (i) supported TiO_2 particles promote the photodegradation process and (ii) the high surface area associated with the small particle size ensures a favourable condition for fast degradation.

4. Conclusion

Nanosized TiO_2-coated cellulose fibres were produced by sol–gel technique at low temperature ($\leq$100 °C), which allows to deposit and to graft TiO_2 nanoparticles. The adopted sol–gel synthesis conditions guarantee the stability of the sol for the industrial application. Under the selected conditions the cellulose fibres are not damaged and titanium dioxide covers uniformly the whole surface of the fibres. On the basis of the results presented before, we can conclude that the thin TiO_2 film constituted by anatase crystallites of about 3–5 nm particle size strongly adhering to the underlying support, is photocatalytically active. It is a matter of fact that the TiO_2-covered cellulose fibres show high photocatalytic efficiency in decomposing the adsorbed MB and heptane-extracted bitumen fraction under solar-like light. The TiO_2 film, although highly efficient in pollutant degradation, does not promote a simultaneous fibre degradation.

Acknowledgments

The authors acknowledge the financial support from Regione Piemonte (Progetto NANOMAT, Docup 2000-2006, Linea 2.4a). M. Jasim Uddin is grateful to Associazione Tessile e Salute for supporting his PhD fellowship.

References

[1] B. Tryba, A.W. Morawski, M. Inagaki, Appl. Catal. B: Environ. 46 (2003) 203–208.
[2] D.F. Ollis, in: H. Al-Ekabi (Ed.), Photocatalytic Purification and Treatment of Water and Air, Elsevier, Amsterdam, 1993.
[3] H. Yamashita, M. Harada, A. Tanii, M. Honda, M. Takeuchi, Y. Ichihashi, M. Anpo, N. Iwamoto, N. Itoh, T. Hirao, Catal. Today 63 (2000) 63–69.
[4] S. Irmak, E. Kusvuran, O. Erbatur, Appl. Catal. B: Environ. 54 (2004) 85–91.
[5] J. Arana, J.M. Dona-Rodriguez, O. Gonzalez-Diaz, E.T. Rendon, J.A.H. Melian, G. Colon, J.A. Navio, J.P. Pena, J. Mol. Catal. A: Chem. 215 (2004) 153–160.
[6] V. Kandavelu, H. Kastien, K.R. Thampi, Appl. Catal. B: Environ. 48 (2004) 101–111.
[7] C.H. Ao, S.C. Lee, J.Z. Yu, J.H. Xu, Appl. Catal. B: Environ. 54 (2004) 41–50.
[8] B.F. Abramovic, V.B. Anderluh, A.S. Topalov, F.F. Gaal, Appl. Catal. B: Environ. 48 (2004) 213–221.
[9] M. Stylidi, D.I. Kondarides, X.E. Verykios, Appl. Catal. B: Environ. 47 (2004) 189–201.
[10] (a) S. Usseglio, P. Calza, A. Damin, C. Minero, S. Bordiga, C. Lamberti, E. Pelizzetti, A. Zecchina, Chem. Mater. 18 (2006) 3412–3424;
(b) M. El Madani, C. Guillard, N. Perol, J.M. Chovelon, M. El Azzouzi, A. Zrineh, J.M. Herrmann, Appl. Catal. B: Environ. 65 (2006) 70–76.
[11] A.G. Rincon, C. Pulgarin, Appl. Catal. B: Environ. 49 (2004) 99–112.
[12] P.J. Li, I. Kangasniemi, K. Degroot, T. Kokubo, J. Am. Ceram. Soc. 77 (1994) 1307–1312.
[13] M. Keshmiri, M. Mohseni, T. Troczynski, Appl. Catal. B: Environ. 53 (2004) 209–219.
[14] F. Xamena, P. Calza, C. Lamberti, C. Prestipino, A. Damin, S. Bordiga, E. Pelizzetti, A. Zecchina, J. Am. Chem. Soc. 125 (2003) 2264–2271.
[15] M. Noorjahan, V.D. Kumari, M. Subrahmanyam, P. Boule, Appl. Catal. B: Environ. 47 (2004) 209–213.
[16] Y. Djaoued, S. Badilescu, P.V. Ashrit, D. Bersani, P.P. Lottici, R. Bruning, J. Sol–Gel Sci. Technol. 24 (2002) 247–254.
[17] A. Matsuda, Y. Kotani, T. Kogure, M. Tatsumisago, T. Minami, J. Am. Ceram. Soc. 83 (2000) 229–231.
[18] W.A. Daoud, J.H. Xin, J. Am. Ceram. Soc. 87 (2004) 953–955.
[19] A. Bozzi, T. Yuranova, I. Guasaquillo, D. Laub, J. Kiwi, J. Photochem. Photobiol. A: Chem. 174 (2005) 156–164.
[20] P.F. Fu, Y. Luan, X.G. Dai, J. Mol. Catal. A: Chem. 221 (2004) 81–88.
[21] F. Bonino, A. Damin, G. Ricchiardi, M. Ricci, G. Spano, R. D'Aloisio, A. Zecchina, C. Lamberti, C. Prestipino, S. Bordiga, J. Phys. Chem. B 108 (2004) 3573–3583.
[22] T. Torimoto, Y. Okawa, N. Takeda, H. Yoneyama, J. Photochem. Photobiol. A: Chem. 103 (1997) 153–157.
[23] Z. Ding, X.J. Hu, G.Q. Lu, P.L. Yue, P.F. Greenfield, Langmuir 16 (2000) 6216–6222.
[24] T. Deguchi, K. Imai, M. Iwasaki, H. Tada, S. Ito, J. Electrochem. Soc. 147 (2000) 2263–2267.
[25] J. Sabate, M.A. Anderson, H. Kikkawa, Q. Xu, S. Cerveramarch, C.G. Hill, J. Catal. 134 (1992) 36–46.
[26] W.A. Daoud, J.H. Xin, Y.H. Zhang, K.H. Qi, J. Non-Cryst. Solids 351 (2005) 1486–1490.
[27] H.C. Choi, Y.M. Jung, S.B. Kim, Vib. Spectrosc. 37 (2005) 33–38.
[28] J. Rockenberger, L. Troger, A. Kornowski, T. Vossmeyer, A. Eychmuller, J. Feldhaus, H. Weller, J. Phys. Chem. B 101 (1997) 2691–2701.
[29] M.A. Marcus, M.P. Andrews, J. Zegenhagen, A.S. Bommannavar, P. Montano, Phys. Rev. B 42 (1990) 3312–3316.
[30] M.A. Moharram, T.Z.A.E. Nasr, N.A. Hakeem, J. Polym. Sci.: Polym. Lett. Ed. 19 (1981) 183–187.
[31] L.S. Birks, H. Friedman, J. Appl. Phys. 17 (1946) 687–692.
[32] J. Molto, R. Font, J.A. Conesa, I. Martin-Gullon, J. Anal. Appl. Pyrolysis 76 (2006) 124–131.
[33] B. Wielage, T. Lampke, G. Marx, K. Nestler, D. Starke, Thermochim. Acta 337 (1999) 169–177.
[34] F. Sandola, V. Balzani, in: N. Serpone, E. Pelizzetti (Eds.), Photocatalysis—Fundamentals and Applications, John Wiley & Sons, New York, 1989.
[35] S.R. Morrison, The Chemical Physics of Surfaces, Plenum, New York, 1977 (Chapter 9).
[36] S. Kutsuna, M. Toma, K. Takeuchi, T. Ibusuki, Environ. Sci. Technol. 33 (1999) 1071–1076.
[37] W. Dechapanya, PhD Thesis, Michigan Technological University, 2002.
[38] C. Lee, Y.W. Sung, J.W. Park, J. Phys. Chem. B 103 (1999) 893–898.
[39] N. Sadlej-Sosnowska, L. Kaczmarek, K. Rotkiewicz, Spectrosc. Acta Pt. A: Mol. Biomol. Spectr. 57 (2001) 199–205.
[40] E. Braswell, J. Phys. Chem. (1968) 2477.